Image Analysis of Porous Media by 3-D Mathematical Morphology

Ulisses de Mendonça Braga Neto[1]
Roberto de Alencar Lotufo[2]

[1]Laboratório de Reconhecimento de Padrões
Departamento de Eletrônica e Sistemas
Universidade Federal de Pernambuco
C.P. 7800 50711-970 Recife, PE
ulisses@npd.ufpe.br

[2]Grupo de Computação de Imagens
Departamento de Engenharia de Computação e Automação Industrial
Faculdade de Engenharia Elétrica
Universidade Estadual de Campinas
C.P. 6101 13081 Campinas, SP
lotufo@dca.fee.unicamp.br

Abstract. This paper presents Mathematical Morphology tools for 3-D image analysis, namely, the geodesic granulometries and the neck histogram. The family of openings which constitutes the geodesic granulometries is parameterized by the radius of the digital disks utilized as structuring elements. We demonstrate the validity of the granulometry thus obtained. The resulting granulometric distributions are determined by the underlying metric associated with the digital disks. Next we propose an algorithm to compute the neck histogram, which is an analysis tool that gives statistical information concerning the occurrence of constrictions in the object studied. Finally we demonstrate the application of the proposed analysis tools in the characterization of a three-dimensional experimental sample designed as a model for a porous medium.

1 Introduction

With the availability of incresingly sophisticated computational resources and imaging equipment in the recent years, 3-D techniques have become a subject of busy research in image processing and analysis. These techniques deal directly with the three-dimensional structure of the real-world objects, without requiring the application of geometric probability concepts, like stereometric correction.

This paper presents Mathematical Morphology tools for 3-D image analysis, namely, the geodesic granulometries and the neck histogram. The application we aimed at is the characterization of porous media, a traditional application of Mathematical Morphology, being of great value in several economically important areas like petrophysics, oil engineering, reservatory engineering, soil analysis and crystalography.

First we present a brief review of concepts related to 3-D Mathematical Morphology, introducing the notation used in the paper and defining some important notions for the forthcoming development, like connectivity and the digital disks.

Then we discuss the geodesic granulometries, which are a classical tool in morphological image analysis. But, unlike the traditional approach, we use as structuring elements for the geodesic openings digital disks according to different metrics, parameterizing the granulometry by the disk radius. We demostrate that this leads to a valid granulometry, which is not true in the case of morphological openings. The geodesic granulometric distributions obtained are determined by the underlying metric associated with the digital disks.

Next we propose an algorithm to compute the neck histogram. This tool, like the granulometries, is based on the "transformation-measure" paradigm of Mathematical Morphology, and gives statistical information concerning the occurrence of constrictions in the object studied.

Finally we show the application of the tools proposed in the analysis of a three-dimensional experimental sample designed as a model for a porous medium. We have based our implementation on the Khoros system. We have used two Khoros toolboxes: MMach, for implementing the Mathematical Morphology operators presented, and V3DTools, for obtaining the renderings displayed in this paper.

2   Notions of 3-D Mathematical Morphology

The first question to be asked about any 3-D image analysis method is which *digital grid* is to be utilized. Unlike the bidimensional case, many 3-D digital grids have been proposed in the literature [11]. We have selected the cubic grid, which despite some difficulties, like the low number of neighbours, is the simplest and most efficient to implement in digital computers and is also perfectly isotropic. The cubic grid is sometimes called the *Voxel* model. The voxels (from *volume element*), are small cubes of uniform size and orientation which form a regular subdivision of 3-D space. We limit our attention to a region of interest, a subset of $\mathbf{Z}^3$, which we will call the voxel space E.

The choice of the digital grid determines the *topology* of the digital 3-D space. The *6-*, *18-* and *26-neighbours* of a given voxel are the voxels which share respectively a face, an edge and a vertice with it. A *path* of length n is a sequence $v_0, v_1, \ldots, v_n$ of voxels in which v_i is a neighbour of v_{i-1} for $i = 1, \ldots, n$. Depending on which neighborhood is considered, we can have 6-, 18- or 26-paths. Let $S \subset E$ and $u, v \in S$ then u and v are *connected* if there is a path starting at u and ending at v lying entirely in S. Given a voxel $v \in E$, the set of voxels connected to it define a *connected component* of S. Obviously, we can define 6-, 18- or 26-connected components of S.

A *distance* is any function $d : E \times E \to \mathbf{R}$ which has the properties of a metric, that is, given any voxels $u, v, w \in E$,

$$d(u,v) \geq 0 \qquad (d(u,v) = 0 \Leftrightarrow u = v) \quad (1)$$
$$d(u,v) = d(v,u) \quad (2)$$
$$d(u,v) \leq d(u,w) + d(w,v) \quad (3)$$

We consider the direct three-dimensional extensions of three well known distances [7]: the city-block, euclidean and chessboard distances, which we denote respectively by d_q, d_e and d_m. It is possible to show that

$$d_m \leq d_e \leq d_q \quad (4)$$

The concept of distance allows us to define *digital disks* in E:

$$D_d(o,r) = \{u \in E \mid d(o,u) \leq r\} \quad (5)$$

where $o \in E$ is the disk center and $r \in \mathbf{Z}^+$, its radius. It follows from eq. 4 that

$$D_{d_q} \subset D_{d_e} \subset D_{d_m} \quad (6)$$

We can see easily that the digital disks associated with the euclidean, city-block and chessboard distances are respectively octahedra, spheres and cubes.

Consider now the set $\mathcal{P}(E)$ of all subsets of E, which is partially ordered by the set inclusion relation $\subset$. The set $(\mathcal{P}(E), \subset)$ provided with the usual union, intersection and complementation set operations is a *complete lattice* [2]. The elements of $\mathcal{P}(E)$ are the objects of interest in the voxel space, and the set inclusion relation expresses the kind of relationship typical to Mathematical Morphology. The mappings between $\mathcal{P}(E)$ and itself are the *binary* morphological operators.

Let $A, B \in \mathcal{P}(E)$, the latter being called a *structuring element*. The binary erosion and dilation operators can be defined respectively as:

$$\epsilon_B(A) = \{u \in E \mid (B + u) \subset A\} \quad (7)$$
$$\delta_B(A) = \bigcup (B + u), \quad \forall u \in A \quad (8)$$

where $B + u$ denotes the translation of B by the voxel u. The binary erosion and dilation are the fundamental operators of binary Mathematical Morphology [1].

3   Geodesic Granulometries

The *granulometries* provide a powerful tool for describing shape and size in image analysis. The method is based on "sieving" of an image followed by measure of the residue left on the sieve. The composition of transformation followed by measure represents the fundamental paradigm of image analysis in Mathematical Morphology [13].

According to Matheron's formalization [10], a family of transformations $\{\psi_\lambda\}$, parameterized by $\lambda \geq 0$ (with $\psi_0(A) = A$) constitutes a granulometry if it is a size criterion, that is, it obbeys Matheron's Axioms:

$$\text{I)} \qquad \psi_\lambda(A) \subset A \quad (9)$$
$$\text{II)} \qquad A \subset C \Rightarrow \psi_\lambda(A) \subset \psi_\lambda(C) \quad (10)$$
$$\text{III)} \quad \psi_\lambda[\psi_\mu(A)] = \psi_\mu[\psi_\lambda(A)] = \psi_{\max(\lambda,\mu)}(A) \quad (11)$$

for all $\lambda, \mu \geq 0$.

Let $A \in \mathcal{P}(E)$ and let $V(\lambda)$ be the number of voxels in $\psi_\lambda(A)$, for $\lambda \geq 0$. For a family $\{\psi_\lambda\}$ satisfying Matheron's axioms, $V(\lambda)$ will be a monoton decreasing function. Further, A being finite entails that $V(\lambda) = 0$ for some $\lambda > \Lambda \in \mathbf{Z}^+$. The function $\Phi : \mathbf{Z}^+ \to \mathbf{R}$ defined as:

$$\Phi(\lambda) = 1 - \frac{V(\lambda)}{V(0)}, \quad \lambda \geq 0 \quad (12)$$

is therefore monoton increasing in the interval $[0, 1]$, so it may be viewed as a cumulative probability distribution. Its associated probability density function

is given by the following discrete derivative:

$$\Gamma(\lambda) = \Phi(\lambda + 1) - \Phi(\lambda), \quad \lambda \geq 0 \quad (13)$$

Due to the properties of $\Phi(\lambda)$ mentioned above, the function $\Gamma(\lambda)$ is non-negative and becomes null for $\lambda > \Lambda$. The functions $\Phi(\lambda)$ and $\Gamma(\lambda)$ are known as the *granulometric distributions* associated with the granulometry. The function $\Gamma(\lambda)$ is also known as the *pattern spectrum*. It is a powerful tool for characterizing shape and size in image analysis [9]. In a manner reminiscent of the Fourier spectrum, it shows the decomposition of a given object in terms of a fundamental shape "scaled" by the increasing values of the parameter λ. So we can define a useful analysis parameter, the *average size*, which is the expected value of the pattern spectrum:

$$\overline{\lambda} = \sum_{\lambda=0}^{\Lambda} \lambda \Gamma(\lambda) \quad (14)$$

Morphological openings $\gamma_{B_\lambda} = \epsilon_{B_\lambda} \delta_{B_\lambda}$ are often used as the transformations ψ_λ. Usually, one starts with a convex primitive structuring element B and then defines B_λ as the composition of $\lambda - 1$ Minkowski sums of B. It is easy to show that this parameterization of the morphological openings follows Matheron's Axioms and constitutes thus a valid granulometry [4]. We call these families of transformations *morphological granulometries*.

However, we would like to use as structuring elements the digital disks defined in section 2 and the disk radius r as the parameterization for the family of transformations. But if we try this with the morphological openings, we run into trouble, for unlike the city-block and chessboard disks, the euclidean disk has not a decomposition in terms of Minkowski sums of a convex primitive structuring element. In fact, the morphological openings by digital euclidean disks, as opposed to the continuous case, do not constitute a granulometry, due to the digitization error associated with the disks. Further, the morphological openings have the well-known effect of distorting the edges of objects in a image, therefore it does not represent a "true" real-world sieve.

So we use instead another class of openings. Let $A, B, C \in \mathcal{P}(E)$. We define the *conditional* dilation of A by the structuring element B, given the *mask* C, as:

$$\delta_{B,C}(A) = \delta_B(A) \cap C \quad (15)$$

The *reconstruction* of A by a set of markers $M \in \mathcal{P}(E)$ is given by:

$$\rho_{B,M}(A) = \delta_{B,A} \left(\delta_{B,A} \left(\ldots (\delta_{B,A}(M)) \ldots \right) \right) \quad (16)$$

where the iterated composition of conditional dilations is performed until stability is achieved. Consider now the reconstruction-based operator given by:

$$\gamma_{B,B_{rec}}(A) = \rho_{B_{rec}, \epsilon_B(A)}(A) \quad (17)$$

where first a erosion of A is performed and the result is used as markers for the reconstruction using the original A as mask. The structuring element B_{rec} expresses the kind of connectivity assumed and is in general different from B. It can be shown that the operator defined in (17) is an opening [14], which we call a *geodesic opening*.

Theorem 3.1 *The family of transformations* $\{\psi_r = \gamma_{B_r, B_{rec}}\}$, $r \geq 0$, *where the structuring elements* $\{B_r\}$ *form a monoton non-decreasing sequence,* $B_s \subseteq B_t$, $t \geq s \geq 0$, *constitutes a valid granulometry.*

Proof. The first two Matheron's axioms are satisfied, for the transformations ψ_r are openings. To prove the third axiom, we note that from the definition of erosion in (7),

$$B_s \subseteq B_t \Rightarrow \epsilon_{B_t}(A) \subseteq \epsilon_{B_s}(A), \quad t \geq s \geq 0 \quad (18)$$

Also, from the definition of the reconstruction operator in (16),

$$M \subseteq N \Rightarrow \rho_{B_{rec}, M}(A) \subseteq \rho_{B_{rec}, N}(A) \quad (19)$$

From (18) and (19) above,

$$\gamma_{B_s, B_{rec}}(A) \subseteq \gamma_{B_t, B_{rec}}(A), \quad t \geq s \geq 0 \quad (20)$$

Now it is a property of the openings [12] that

$$\gamma_t(A) \subseteq \gamma_s(A) \Leftrightarrow \gamma_t[\gamma_s(A)] = \gamma_s[\gamma_t(A)] = \gamma_t(A) \,(21)$$

From (20) and (21), the third axiom is satisfied. □

We call the above families of transformations *geodesic granulometries*. As a corolary from Theorem 1, we can use digital disks, *including* the euclidean disk, as structuring elements for geodesic granulometries, for they always form a monoton non-decreasing sequence. In this way we obtain geodesic granulometric distributions $\Phi(r)$ and $\Gamma(r)$ as a function of the digital disk radius, and also an *average radius* as the expected value of the geodesic pattern spectrum.

We remark that there is a result by Heijmans [8][prop. 9.50] which states that if a family of transformations is a granulometry, then the family of the same transformations folowed by reconstruction is also a granulometry. Now even if we replaced the erosion by a morphological opening in eq. (17), which

would be a equivalent definition of the geodesic opening, obviously we could not use Heijman's proposition to arrive at theorem 1. For instance, the morphological openings by digital disks *do not*, in general, constitute a granulometry in the first place.

Note that the use of digital disks as structuring elements for the geodesic granulometries allows us to have a very natural concept of discrete size, which is induced by the underlying metric associated with the digital disks. In fact, we can speak of cityblock, euclidean or chessboard geodesic granulometric distributions. Further, we get rid of the annoying edge-distorting effect presented by the morphological granulometries, for the geodesic opening represents a pure "cleaning" operation, removing some objects but leaving the rest unaltered. In this sense, the geodesic granulometries approach a true real-world sieving operation.

However, the trade-off is that the geodesic openings are sensitive to the *connectivity* of the objects. To cope with this problem, we must do the *binary segmentation* of the image, disconnecting the overlapping objects. Towards this, we make use of the *geodesic watershed* method [14, 16].

We will illustrate these concepts with a two-dimensional image, a planar section of the 3-D experimental sample studied in section 5. In fig. 1, we see the original image, showing several overlapping particles, the manually obtained markers for the geodesic watershed method superposed in the original image and the resulting segmented image. In fig. 2, we utilize the same image as in fig. 1 to illustrate the edge-distorting effect of the morphological opening, contrasting it to the information-preserving geodesic opening. Note that applying the geodesic opening to the original unsegmented image yields a useless result.

4   Neck Histograms

The *neck histogram* is a statistical distribution which indicates the occurence of *necks* in a object as a function of a size parameter. The neck histogram, like the granulometric distributions, is an analysis tool that follows the fundamental paradigm of transformation-measure of Mathematical Morphology.

By *neck* we mean a constriction in a connected component. Now an erosion by a sufficiently large strucutring element can detect such constrictions, as we can see in fig. 3. We prefer to use erosions rather than openings, not only because the former are less expensive computationally, but also because they are more convenient for the algorithm to build the neck histogram we propose, as it will be seen.

The concept of digital size we utilize is the same

of the morphological granulometries mentioned in section 3. Starting from a primitive structuring element $B \in \mathcal{P}(E)$ we say that sB, defined by

$$sB = \begin{cases} o \text{ (origin)}, & s = 0 \\ B, & s = 1 \\ \underbrace{B \oplus \ldots \oplus B}_{s-1 \text{ times}}, & s \geq 2 \end{cases} \quad (22)$$

has size s (where the operator $\oplus$ denotes the Minkowski sum). Now it is a well-known property of erosions that

$$\epsilon_{B_1} \epsilon_{B_2} \cdots \epsilon_{B_n} = \epsilon_{B_1 \oplus B_2 \oplus \ldots \oplus B_n} \quad (23)$$

so that successive erosions by the same fundamental structuring element B is equivalent to a single erosion by sB.

The outline of an algorithm to compute the neck histogram is then to perform successive erosions by a given primitive structuring element and *count* the number of connected components left after each erosion, obtaining thus a cumulative distribution $\Omega(s)$ as a function of the size s of the necks detected at each step. Much in the same way as the pattern spectrum, the neck histogram is then found by computing the discrete derivative of the cumulative distribution:

$$\Upsilon(s) = \Omega(s + 1) - \Omega(s), \quad s \geq 0 \quad (24)$$

Also, the expected value of the neck histogram yields the *average neck size*:

$$\bar{s} = \frac{\sum_{s=0}^{S} s \, \Upsilon(s)}{\sum_{s=0}^{S} \Upsilon(s)} \quad (25)$$

Note that different neck histograms, conveying sometimes complementary information, can be obtained by varying the fundamental structuring element B.

The counting is performed by taking the maximum value of the *labelled* image after each erosion. Letting $A \in \mathcal{P}(E)$, we define the labelling transformation as:

$$\text{lab}(A)(u) = \begin{cases} 0 & \text{if } u \in A^c \\ l & \text{if } u \in l\text{-th conn. comp.} \end{cases} \quad (26)$$

for all $u \in E$, where $l \geq 1$ is the label given to each connected component. The neighborhood used in the labelling algorithm determines which connectivity (6, 18 or 26) is assumed, which must be the same as the one used in the reconstruction step of the geodesic opening.
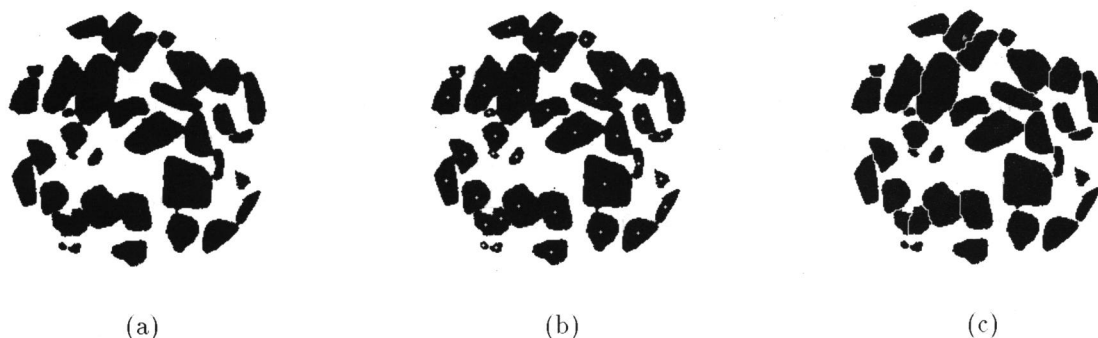
(a)   (b)   (c)

Figure 1: Binary segmentation via geodesic watersheds: (a) original image (b) manual markers superposed to original image (c) segmentation result

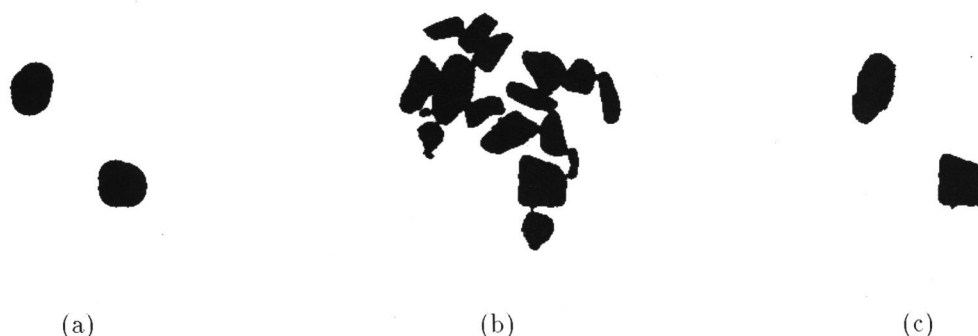(a)   (b)   (c)

Figure 2: Openings by a euclidean digital disk of radius $r = 15$: (a) morphological opening of original image (b) geodesic opening of original image (c) geodesic opening of segmented image
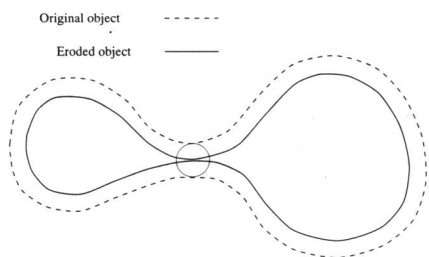

Original object   - - - - - -
Eroded object   ———

Figure 3: Object about to disconnect after erosion by the largest disk inscribable in the neck

Now a very important detail is that we cannot afford to let any component disappear after an erosion at any step, for then the counting would obviously cease to give the number of necks detected. (The cumulative distribution $\Omega(s)$ might even turn decreasing, producing negative values in the neck histogram!). So we must utilize *conditional erosions* which are defined analogously to the conditional dilations in eq. (15):

$$\epsilon_{B,C}(A) = \epsilon_B(A) \cup C \qquad (27)$$

where the mask C is the set of components that would disappear after an erosion of size s. Note that there is no such thing as a "conditional opening", and that is one of the reasons why the algorithm is based on erosions.

To find the mask for the conditional erosion we make use of the geodesic opening defined in eq. (17): the difference between the original set and its geodesic opening by the primitive structuring element B yields the components that would vanish after the erosion by B. We call this operator a *geodesic top-hat*:

$$\xi_B = I - \gamma_{B,B_{rec}} \qquad (28)$$

The result of the geodesic top-hat is used at each step as mask for the conditional erosion. After a finite number of steps, the eroded image becomes equal to the mask, and the algorithm stops. Note that the use of erosions instead of openings allows us to have this convenient stopping criterion.

The pseudo-code in the next page implements the algorithm for computing the neck histogram we have proposed in this section.

- Data:

  - L, Input binary image
  - M, Work image to store the mask
  - g[ ], Array to store the accumulated distribution $\Omega(s)$
  - h[ ], Array to store the neck histogram $\Upsilon(s)$

- Accumulated distribution $\Omega(s)$ computation:
  For $i \leftarrow 0, 1, 2, \ldots$
    g[i] $\leftarrow$ max $\{lab(L)\}$
    $M \leftarrow \xi_B(L)$
    $L \leftarrow \epsilon_{B,M}(L)$
    If $(L = M)$ exit loop;
      Else, go through the loop again

- Neck histogram $\Upsilon(s)$ computation:
  For $i \leftarrow 0, 1, 2, \ldots, S - 1$
    h[i] $\leftarrow$ g[i+1] - g[i]

5 Experimental Results: 3-D Analysis of a Porous Medium

In this section we demonstrate the application of the proposed 3-D analysis tools in the analysis of a three-dimensional experimental sample, an artificial model of a porous medium. The experimental sample is an aproximately cylindrical object made of plaster with small chalk pieces of several sizes and shapes inserted in it. The highly packed chalk pieces are intendend to model the *solid* phase of a porous medium, which is the material itself, whereas the plaster plays the role of the *porous* phase, the open spaces through which fluids can flow altering the physical properties of the medium.

We have implemented the described 3-D analysis tools on the Khoros image processing platform. This system is an open package developed at New Mexico University and freely available through anonymous ftp. We have based our implementation on the MMach Khoros toolbox [3], also available through anonymous ftp at São Paulo University. We have extended the MMach toolbox to handle 3-D data sets, adding new subroutines for implementing three-dimensional dilation, erosion, watershed, labelling and distance function and reconstruction operators. Most of these subroutines are based on FIFO queue algorithms, which are very convenient to implement multidimensional morphological operators.

We have sectioned the experimental sample and acquired each slice using a common scanner. Then we have employed an original registration method [5, 6] to bring the slices into alignment. After a segmentation step, we have interpolated the sections as-

sociated with the porous and solid phases. The output of the above 3-D reconstruction procedure was the two binary volumes rendered in fig. 4.

The 3-D binary segmentation of the solid phase required for applying the geodesic granulometries was a difficult step, due to the high compactness of the chalk pieces representing the grains in the solid phase. We have employed the geodesic watershed method, using as markers for the segmentation the regional maxima of a filtered version of the 3-D distance function [15]. In fig. 5 we see the geodesic pattern spectra and associated average radii of the solid phase obtained by utilizing the digital disks defined in section 2. The geodesic pattern spectra give information on the morphological structure of the constituent grains of the solid phase. As pointed out in section 3, the sizes measured by the geodesic pattern spectra are determined by the underlying metric associated with each digital disk. In fact, we can see that the maximum value of the spectra as well as the average radii are decreasing, as would be expected from eq. (4).

Next we applied the algorithm proposed in section 4 to compute the neck histograms and associated neck average sizes of the solid and porous phases, which we see in figs. 6 and 7, respectively. The characterization of the neck distribution in a porous medium is very useful, for it indicates the degree of opposition the medium offers to percolation by fluids. We have used as primitive structuring elements the city-block and chessboard digital disks of radius 1, which are respectively the $3 \times 3 \times 3$ "3-D cross" and cube. Since the composition sB of these primitive structuring elements gives rise to the respective digital disks of radius s, the neck histograms computed, like the geodesic pattern spectra of fig. 5, can be said to be function of the underlying metric.

6 Conclusion

In this work we have proposed Mathematical Morphology tools for 3-D image analysys. The use of digital disks as structuring elements enabled us to get geodesic granulometries which are determined by the underlying metric associated with the disks. We have presented also an algorithm to compute the neck histogram, a tool which gives statistical information concerning the occurrence of constrictions in the object studied. We demostrated the application of the tools proposed in the characterization of a 3-D experimental sample designed as a model of a porous medium.

The metrics associated with the digital disks need not be limited to the city-block, euclidean and chessboard. Other choices may lead to interesting re-

(a) (b)

Figure 4: Rendering of the binary (a) porous phase (b) solid phase after 3-D reconstruction

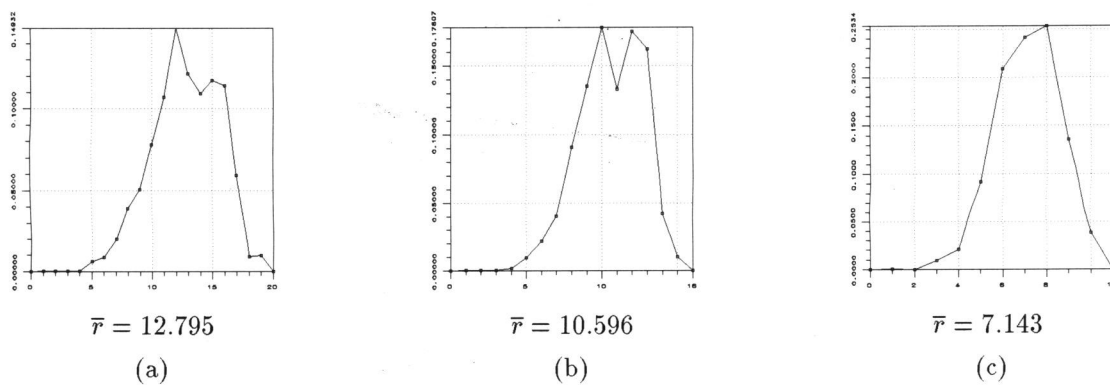$\bar{r} = 12.795$ $\bar{r} = 10.596$ $\bar{r} = 7.143$

(a) (b) (c)

Figure 5: (a) City-block, (b) euclidean and (c) chessboard pattern spectra and associated average radii of the solid phase

sults, offering new interpretation of the granulometric distributions. The use of other kinds of digital grids may also improve some critical issues, like the 3-D binary segmentation required by the geodesic granulometries.

Acknowledgements

References

[1] G.J.F. Banon and J. Barrera. Minimal representations for translation-invariant set mappings by mathematical morphology. *SIAM J. Appl. Math*, 51(6):1782–1798, Dec 1991.

[2] G.J.F. Banon and J. Barrera. Decomposition of mappings between complete lattices by mathematical morphology, Part I. General lattices. *Signal Processing*, 30:299–327, 1993.

[3] J. Barrera, G.J.F. Banon, and R.A. Lotufo. A Mathematical Morphology toolbox for the KHOROS system. Technical Report RT-MAC-9403, Instituto de Matemática e Estatística - Universidade Estadual de São Paulo, São Paulo, SP, Brasil, Jan 1994.

[4] U.M. Braga Neto. *Reconstrução Volumétrica e Análise de Imagens Tridimensionais por Morfologia Matemática*. MSc thesis, State University of Campinas, Brazil, 1994.

[5] U.M. Braga Neto and R.A. Lotufo. A computationally eficient technique for the registration of serial sections (In portuguese). In *Proceedings of SIBGRAPI'94 - VII Brasilian Symposium of Computer Graphics and Image Processing*, Curitiba, PR - Brazil, Nov 1994.
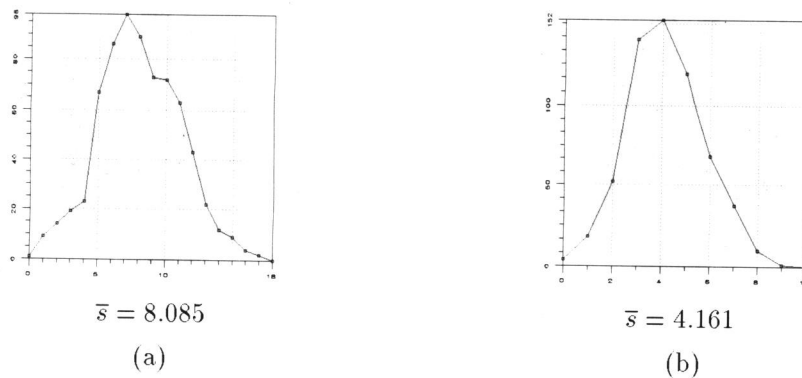
$\bar{s} = 8.085$

(a)

$\bar{s} = 4.161$

(b)

Figure 6: Neck histograms and associated average sizes of the solid phase using as primitive structuring element (a) the $3 \times 3 \times 3$ "3-D cross" and (b) the $3 \times 3 \times 3$ cube

$\bar{s} = 5.579$
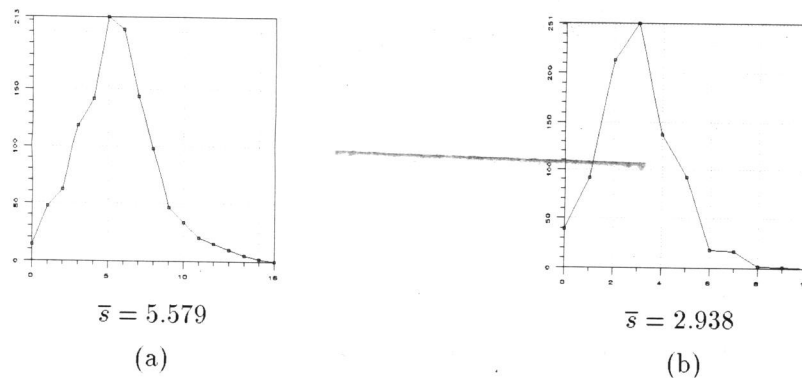
(a)

$\bar{s} = 2.938$

(b)

Figure 7: Neck histograms and associated average sizes of the porous phase using as primitive structuring element (a) the $3 \times 3 \times 3$ "3-D cross" and (b) the $3 \times 3 \times 3$ cube

[6] U.M. Braga Neto and R.A. Lotufo. A new efficient technique for the registration of serial sections. *CVGIP: Graph. Models. and Image Proces.*, Dec 1994. Submitted.

[7] R.C. Gonzalez and R.E. Woods. *Digital Image Processing*. Addison Wesley Publishing Co., 2nd edition, 1992.

[8] H.J.A.M. Heijmans. *Morphological Image Operators*. Academic Press, Inc., 1994.

[9] P. Maragos. Pattern spectrum and multiscale shape representation. *IEEE Transactions on Pat. Anal. Mach. Intel.*, 11(7):701–716, jul 1989.

[10] G. Matheron. *Random sets and integral geometry*. Wiley, New York, 1975.

[11] F. Meyer. Mathematical morphology: from two dimensions to three dimensions. *Journal of Microscopy*, 165(1):5–28, Jan 1992.

[12] C. Ronse and H.J.A.M. Heijmans. The algebraic basis of mathematical morphology. Part II: openings and closings. *CVGIP: Image Understanding*, 54:74–97, 1991.

[13] J. Serra. *Image analysis and mathematical morphology*. Academic Press, Inc., 1982.

[14] J. Serra and L. Vincent. Morphological filtering. In *EURASIP course: "Median and Morphological Filtering in Image and Signal Processing"*, Tampere, Finland, Jun 1989.

[15] L. Vincent. Morphological grayscale reconstruction in image analysis: Applications and efficients algorithms. *IEEE Transactions on Image Processing*, 2(2):176–201, Apr 1993.

[16] L. Vincent and P. Soille. Watersheds in digital spaces: an efficient algorithm based on immersion simulations. *IEEE Transactions on Pat. Anal. Mach. Intel.*, 13(6):583–598, Jun 1991.